KeA1

CHINESE ROOTS
GLOBAL IMPACT

Contents lists available at ScienceDirect

Petroleum Science

journal homepage: www.keaipublishing.com/en/journals/petroleum-science



Original Paper

Syntheses and properties of associative acrylamide copolymers containing short hydrophobic chains used in a friction reducer for slick-water fracturing



Ya-Xing Dai ^{a, b}, Xian-Li Zhang ^a, Si-Yuan Liu ^a, Feng-Run-Ze Zhang ^a, Yi-Xi Zhang ^a, Yu-Tong Sang ^a, Jing-Xi Zheng ^a, Zhao-Sheng Liu ^c, Peng Zhang ^{a, *}

- ^a College of Chemistry and Chemical Engineering, Chongqing University of Science and Technology, Chongqing, 401331, China
- ^b College of Ecology and Environment, Chongqing Resources and Environmental Protection of University, Chongqing, 401331, China
- ^c China Property Project Department of Dezhou, Mining Property Service Center, Shengli Oilfield Company of Sinopec, Dezhou, 253000, Shandong, China

ARTICLE INFO

Article history: Received 21 May 2023 Received in revised form 19 March 2024 Accepted 19 March 2024 Available online 26 March 2024

Edited by Yan-Hua Sun

Keywords: Shale gas Slick water Drag reducer Modified monomer Copolymerization

ABSTRACT

Two allyldimethylalkyl quaternary ammonium salt (AQAS) monomers, N,N-dimethylallylphenylpropylammonium bromide (AQAS1) and N,N-dimethylallylnonylammonium bromide (AQAS2), were synthesized and used to prepare modified polyacrylamide materials. Two new drag reducers were synthesized from acrylamide (AM), sodium acrylate (NaAA) and a cationic modified monomer (AQAS1 or AQAS2) via aqueous solution polymerization, and the copolymers were named P(AM/NaAA/AQAS1) and P(AM/NaAA/ AQAS2), respectively. The structures of the drag reduction agents were confirmed by IR and ¹H NMR spectroscopies. The molecular weight ($M_{\rm w}$) of P(AM/NaAA/AQAS1) was 1.79 imes 10⁶ g/mol. When the copolymer concentration was 1000 mg/L and the flow rate was 45 L/min, in fresh water the highest drag reduction rate was 75.8%, in 10,000 mg/L NaCl solution the drag reduction rate decreased to 72.9%. The molecular weight of P(AM/NaAA/AOAS2) was 3.17×10^6 g/mol. When the copolymer concentration was 500 mg/L and the flow rate was 45 L/min, the drag reduction rate reached 75.2%, and in 10,000 mg/L NaCl solution the drag reduction rate was 73.3%, decreased by approximately 1.9%. The drag reduction rate for partially hydrolyzed polyacrylamide (HPAM) was also investigated, and the results showed that the drag reduction rates for 500 and 1000 mg/L HPAM solutions were merely 43.2% and 49.0% in brine, respectively. Compared with HPAM, both of the above copolymers presented better drag reduction capacities. © 2024 The Authors. Publishing services by Elsevier B.V. on behalf of KeAi Communications Co. Ltd. This is an open access article under the CC BY-NC-ND license (http://creativecommons.org/licenses/by-nc-nd/ 4.0/).

1. Introduction

With the immoderate exploitation of traditional reservoirs, unconventional natural oil and gas reservoirs, such as low-permeability shale gas reservoirs, have attracted wide attention (Li et al., 2022a; Kerimov et al., 2016; Nakamura et al., 2019). Due to the low permeabilities of shale gas reservoir rocks, hydraulic fracturing technology is the main treatment used to enhance shale gas recovery and meet commercial demand (Xing et al., 2020; Ibrahim et al., 2018). Furthermore, a drag reducer (DR) is required to reduce the flow resistance and energy consumption (Chen et al., 2020; Wei

 $\label{lem:compact} \textit{E-mail} \quad \textit{addresses} : \quad \texttt{zhangpeng@cqust.edu.cn,} \quad \texttt{zhangpengchina@foxmail.com} \ (P. \, Zhang).$

et al., 2022; Zhao et al., 2018). In field applications, a greater injection rate means a greater shear force (Yu et al., 2022), and a high-speed liquid in the pipe could induce polymer chain degradation, considerable energy loss and decreases in the drag reduction rate of the DR (Soares, 2020; Kim et al., 1974). Moreover, the high salinities of flowback fluids are also of concern (Zeng et al., 2020), and the reuse of flowback fluids is expected to reduce freshwater consumption (Nguyen et al., 2018). Therefore, in field applications, the above status requires that the drag reducer must have excellent salt tolerance and high shear resistance.

To date, natural polysaccharides (guar gum, xanthan gum and so on) (Li et al., 2022b; dos Santos et al., 2020; Tian et al., 2015), surfactants (Lin et al., 2001; Tamano et al., 2010), polyethylene oxide (PEO) (Dai et al., 2021), polyacrylamide (Ge et al., 2021; Jing et al., 2021) and composite systems (Gu et al., 2020; Habibpour and Clark, 2017) have been used as drag reducers in different fields.

^{*} Corresponding author.

However, in reality, hydrophobic associated polymers are the most widely used drag reducing agents, and they exhibit excellent drag reduction performance (Chen et al., 2021). Usually, there are more than 10 carbons in the chains of the hydrophobic groups, such as N,N-dodecylacrylamide (C₁₂AM) and N,N-di-n-dodecylacrylamide (DiC₁₂AM) (Tan et al., 2020), dodecyl 2-methylacrylate (DM) (Ma et al., 2019), alkyl acrylamide (carbon number 16) (Wang et al., 2016) and 1-chlorohexadecane (Guo. 2021). However, the long hydrophobic chains inevitably limit the solubility of the polymer. Thus, to enhance the solubilities of polymers, added polar groups (acrylate (NaAA) or 2-acrylamide-2-methyl propane sulfonic acid (AMPS)) might cause the hydrophobically associative polyacrylamide to exhibit excellent solubility (Yang et al., 2019); additionally, by reducing the carbon chain of the hydrophobic groups, the solubility of the polymer can also be increased. Therefore, polar groups and short hydrophobic chain monomers were used in this work to modify polyacrylamide, and the copolymer showed both associative ability and good solubility, as expected.

Two allyldimethylalkyl quaternary ammonium salt monomers were synthesized, which exhibited different hydrophobic structures. Using aqueous solution polymerization, two novel copolymers were synthesized, P(AM/NaAA/AQAS1) and P(AM/NaAA/ AQAS2), and both of the copolymers were based on AM, NaAA and modified monomers (AQAS1 or AQAS2). The optimal polymerization conditions for the copolymers were investigated, the critical association concentrations (CACs) and molecular weights were determined, FTIR spectroscopy and nuclear magnetic resonance spectrometry were utilized to confirm the structures of the products, and the microscopic morphology of the copolymer solution was observed with scanning electron microscopy (SEM). In addition, the effects of shear rate and salinity on the viscosity of the copolymer solution were probed separately, and the rheological properties of the copolymer solution were measured. Finally, the drag reduction effects of the copolymers were tested.

2. Materials and methods

2.1. Materials

Acrylamide (AM) (AR, Chengdu Kelong Chemical Co., Ltd.), acrylic acid (AA) (AR, Chengdu Kelong Chemical Co., Ltd.), sodium hydroxide (NaOH) (AR, Chengdu Kelong Chemical Co., Ltd.), urea (AR, Chengdu Kelong Chemical Co., Ltd.), N,N-dimethylallylamine (ADMA) (98%, Shanghai Macklin Biochemical Co., Ltd.), 1-bromo-3-phenylpropane (98%, Shanghai Aladdin Reagent Co., Ltd.), 1-bromononane (98%, Shanghai Aladdin Reagent Co., Ltd.), 2,2'-azo-bis(2-methylpropionamidine) dihydrochloride (V50) (CG, Shanghai Macklin Biochemical Co., Ltd.), acetone (AR, Chongqing Chuandong Chemical Co., Ltd.), petroleum ether (AR, Chongqing Chuandong Chemical Co., Ltd.), NaCl (AR, Chengdu Kelong Chemical Co., Ltd.), CaCl₂ (AR, Chengdu Kelong Chemical Co., Ltd.) were obtained from the indicated suppliers.

2.2. Syntheses and characterizations of the cationic modified monomer and the DR agent

ADMA and 1-bromo-3-phenylpropane were added to a three-necked flask ($n_{\rm ADMS}$: $n_{1\text{-bromo-3-phenylpropane}}=1.1:1$) containing 50 g of acetone as the solvent, and the quaternization reaction was run for 24 h at 50 °C. The product was poured into a partitioning funnel and extracted 3 times with petroleum ether (60–90 °C boiling range). Finally, AQAS1 was obtained, and the synthetic method for AQAS2 was the same as that for AQAS1. The synthetic routes to the cationic-modified monomers are shown in Scheme 1.

Aqueous solution polymerization was used to synthesize the DR

agent. AM, NaAA and the cationic modified monomer were added to a three-neck flask, and then urea was added with distilled water. This system was kept under nitrogen for 30 min, and then the initiator (V50) was added to the three-neck flask. The copolymer was polymerized for 5 h at various temperatures (35–55 °C), and HPAM was prepared from AM and NaAA ($n_{\rm AM}$: $n_{\rm NaAA}=3:1$). The synthetic routes to the two drag reducing agents are shown in Scheme 2.

The infrared (IR) spectra of the copolymers were measured with KBr pellets, and the infrared spectra of modified monomers were measured in liquid films with a Bruker Tensor FTIR spectrometer (Bruker, Germany). ¹H NMR spectra of the products were determined with an Agilent 400-MR DD2 nuclear magnetic resonance instrument.

2.3. Properties of the copolymer solutions

2.3.1. Intrinsic viscosity and molecular weight

The intrinsic viscosity of the copolymer solution was measured at 30 °C with a Ubbelohde viscometer and the dilution method, the intrinsic viscosity $[\eta]$ was determined by fitting a linear plot of inherent viscosity versus mass concentration; the intercept of the plot was the intrinsic viscosity, and the molecular weight (M) was calculated with Eq. (1) (Pu et al., 2016).

$$M = \left(\frac{[\eta]}{K}\right)^{\frac{1}{\alpha}} \tag{1}$$

where M represents the molecular weight, g/mol; $[\eta]$ represents the intrinsic viscosity, mL/g; K is a constant value, $K = 4.75 \times 10^{-3}$; and α is constant value, $\alpha = 0.8$.

2.3.2. Apparent viscosities of the copolymers

The apparent viscosity of the copolymer solution was tested with a Brookfield DV2T viscometer (ULA [0] rotor) at room temperature.

2.3.3. Microstructural analyses

The copolymers were dissolved in distilled water and lyophilized after rapid cooling with liquid nitrogen. Then, scanning electron microscopy (SEM) was used to characterize the microstructures of the copolymers.

2.3.4. Rheological properties of the ternary copolymers

The rheological properties of the copolymer solution were determined at room temperature with an MCR102 Anton Paar rheometer. Copolymer solutions were prepared with different concentrations: 1000, 3000, and 5000 mg/L. The stresses of the copolymers were measured from 0.1% to 10,000% to determine the relationships between the elastic modulus (G') and viscous modulus (G') at various concentrations. Frequency sweeps of the copolymers were measured from 0.1 to 100 rad/s to determine how the viscoelasticity of the copolymer solution changed.

2.4. Copolymer performance test

The salt resistance of the copolymer solution was tested by increasing the NaCl concentration from 0 to 10,000 mg/L, and the apparent viscosity of the copolymer solution was measured with a Brookfield DV2T viscometer (ULA [0] rotor) at room temperature. The shear resistance of the copolymer solution was measured at room temperature with an MCR102 Anton Paar rheometer. A HAMZ-IV friction instrument (Fig. 1) was used to measure the copolymer solution drag reduction rate, which was prepared with

Scheme 1. Synthetic routes to the cationic modified monomers.

Scheme 2. Synthetic routes to the two drag reduction agents.

fresh water or brine (NaCl, 10,000 mg/L). The flow rate was 20-45 min/L, and the copolymer solution concentrations were 500-1500 mg/L. The pressures (P) of different situations were recorded. The DR performance of the copolymer was calculated with Eq. (2).

$$R = \frac{P_1 - P_2}{P_1} \times 100\% \tag{2}$$

where R is the drag reduction rate of the copolymer solution, %; P_1 is the pressure of the fresh water or brine, kPa; and P_2 is the pressure of the copolymer solution, kPa.

3. Results and discussion

3.1. Characterization of cationic modified monomers and acrylamide copolymers

The structures of cationic modified monomers and ternary copolymer were characterized by IR spectroscopy, as shown in Fig. 2. In the FT-IR spectrum (Fig. 2(a)), the peaks at 3405, 3030, and 1640 cm⁻¹ indicated stretching vibrations of C–N, C–H (bonds in benzene ring) and C=C bonds in AQAS1, and the peak at 1475 cm⁻¹ represented the C–H bending vibrations of AQAS1. The peaks at 1640 and 1425 cm⁻¹ corresponded to C=C stretching modes, that at 2854 cm⁻¹ was for $-\text{CH}_2$ - stretching modes, and the absorption band for $(\text{CH}_2)_n$ (n > 4) usually appears at 720 cm⁻¹. The functional groups were confirmed with the FT-IR spectra of (P(AM/NaAA/))

AQAS1) and P(AM/NaAA/AQAS2). The N—H absorptions of the copolymers usually appear at approximately $3400-3300 \text{ cm}^{-1}$, the peaks at 1680 and 3089 cm⁻¹ indicated stretching vibrations of P(AM/NaAA/AQAS1), and that at 724 cm⁻¹ was the absorption band for the (CH₂)_n (n > 4) segments of P(AM/NaAA/AQAS2).

Fig. 3 shows the ¹H NMR spectra of the cationic modified monomers and ternary copolymer, respectively. For AQAS1, the signal at 3.32–3.26 ppm was due to the protons of N–CH₂– (d); the protons of $-N-(CH_3)_2$ (e) appeared at 3.03-3.00 ppm; the signal at 4.01-3.98 ppm was assigned to CH₂ protons (f); the signal for =CH- protons (g) appeared at 6.06-5.97 ppm; the CH₂= protons (g) appeared at 5.65–5.58 ppm; the Ph protons (a) appeared at 7.34–7.20 ppm; the –CH₂– protons (b) near Ph groups appeared at 2.63-2.58 ppm; and the phenyl protons (c) appeared at 2.06-2.00 ppm. For AQAS2, the peaks at 0.89-0.85 ppm represented -CH₃ groups (a), the protons of the straight chains -CH₂groups (b) were observed at 1.32–1.24 ppm, and the peaks at 1.73-1.63 and 3.26-3.20 ppm were for $-CH_2-(c)$ and $-(CH_2)-(d)$ protons, respectively. Fig. 3(b) shows a signal at 2.24–1.85 ppm for the -CH- groups (c) in the main chain, the -CH₂- groups in the main chain (b) also resonated at 1.72–1.15 ppm, and the peaks at 7.31–7.14 ppm were for phenyl protons (a) and the signals at 3.68-3.62 ppm indicated $-N-(CH_3)_2$ groups (d). Fig. 3(c) shows a signal at 0.75-0.68 ppm for the $-CH_3$ groups (a), and the signals for $-N-(CH_3)_2$ protons (d) appeared at 3.72-3.59 ppm. Generally, these materials can be identified as the targeted products.

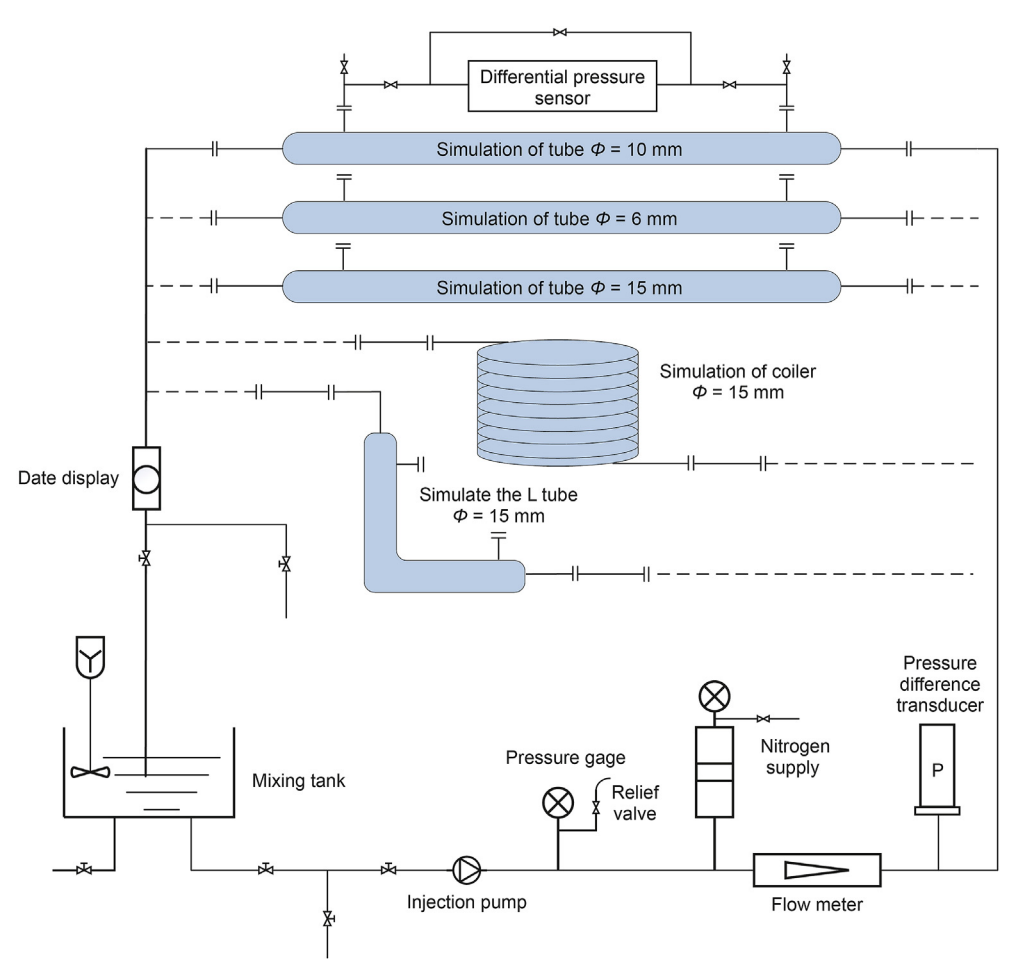


Fig. 1. Fracturing fluid fractionation instrument and the pipeline flow chart.

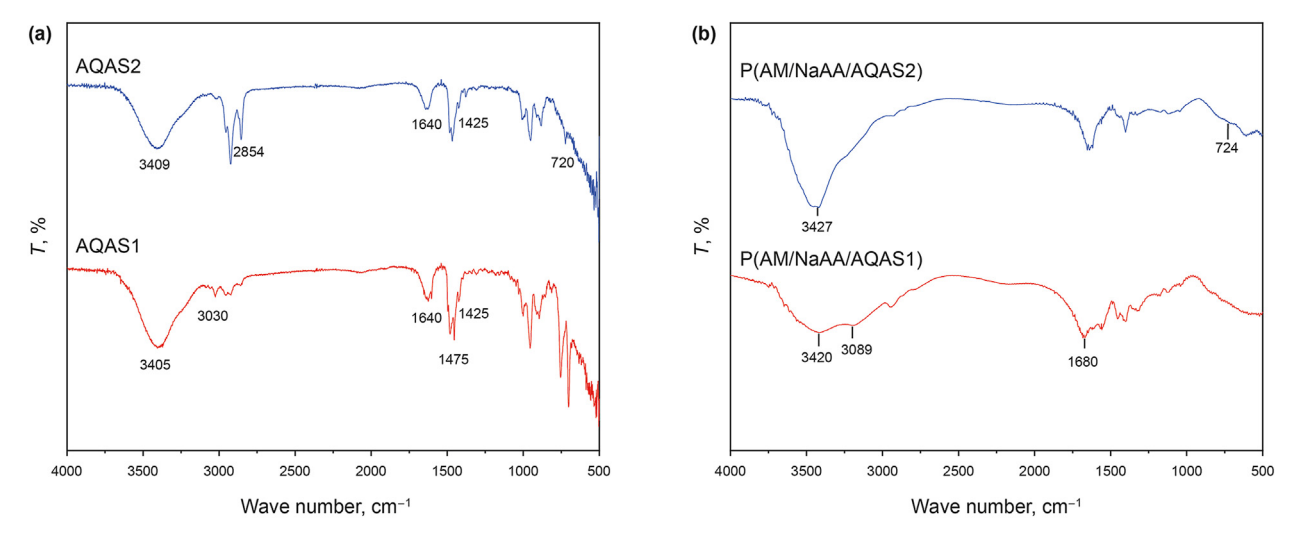
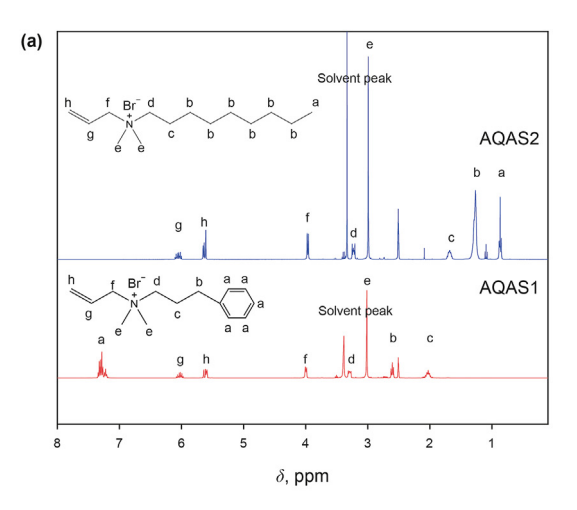


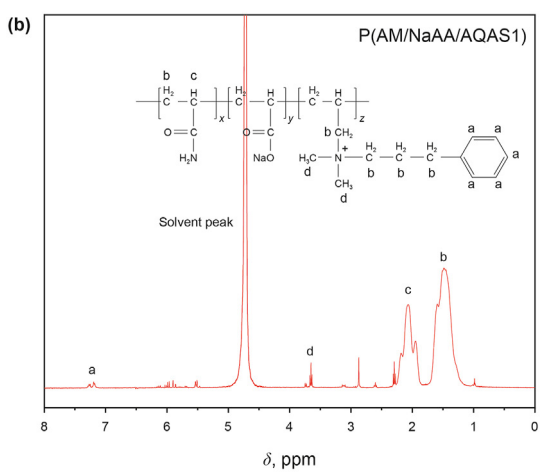
Fig. 2. FT-IR spectra of cationic modified monomers (a) and copolymers (b).

3.2. Effect of the synthetic conditions on the apparent viscosity

The effects of the synthetic conditions on the apparent viscosities are shown in Fig. 4. With increasing total monomer content, the viscosities of P(AM/NaAA/AQAS1) and P(AM/NaAA/AQAS2) both increased. When the total monomer content reached 35 wt%,

the apparent viscosity of the system reached a maximum, and then the apparent viscosity decreased as the total monomer content increased, as shown in Fig. 4(a). These results indicated that when the total monomer content was maintained at a low value, the free radicals did not react with the monomer efficiently, however, excess monomer required a higher temperature and a faster





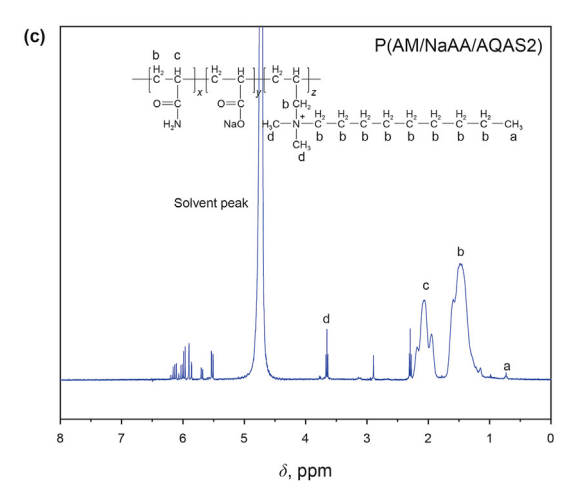


Fig. 3. 1 H-NMR spectra of the cationic modified monomers (DMSO-d $_{6}$ solution) (**a**) and copolymers (D $_{2}$ O solution) (**b**, **c**).

polymerization rate for the system, so the apparent viscosities of the copolymers were reduced.

As shown in Fig. 4(b), the apparent viscosity of P(AM/NaAA/AQAS1) increased as the AQAS1 concentration was increased, reached a maximum at 0.5 mol%, and then the apparent viscosity decreased slowly, which meant that when the concentration of AQAS1 remained low, the concentrations of the hydrophobic groups were low, and the hydrophobic association process was not

complete. Then, above 0.5 mol%, the apparent viscosity suddenly decreased, which may have occurred because mutual repulsions between the charges affected the continuous free radical polymerization and led to a decrease in the apparent viscosity of the copolymer. The apparent viscosity of P(AM/NaAA/AQAS2) decreased obviously with increasing AQAS2 concentration. These results indicated that with the same number of carbon atoms, the linear structures increased the viscosity more efficiently than the ring structures and achieved the highest viscosity at a low dosage.

Different concentrations of the initiator were also investigated, and Fig. 4(c) shows that 0.3 wt% and 0.1 wt% were the best concentrations for P(AM/NaAA/AQAS1) and P(AM/NaAA/AQAS2), respectively. With increasing initiator content, the apparent viscosity of P(AM/NaAA/AQAS1) first increased to 441.8 mPa s (0.3 wt%) and then decreased to 328.9 mPa s (0.1 wt%). However, for P(AM/NaAA/AQAS2), it seems that polymerization occurred more easily with low initiator concentrations and reached the highest apparent viscosity at 0.1 wt%.

Fig. 4(d) shows clearly that the apparent viscosity of the copolymer solution was almost unaffected by urea. In this experiment, the solubilities of both copolymers were excellent, and it was difficult to determine the solubilities with various urea contents, so 1 wt% was selected.

The polymerization reactions were strongly dependent on the temperature, as shown in Fig. 4(e). The best reaction temperature for both copolymers was 35 °C, and the apparent viscosities decreased with increasing temperature. This indicated that many primary radicals were produced at the higher temperatures, the polymerization reaction rates were increased, and the chain transfer rates were greater than the chain growth rates. Additionally, the polymerizations were exothermic reactions, and high temperatures generate high chain transfer rates; this results in burst polymerization and sharp decreases in the polymer molecular weight and apparent viscosity of the solution. Therefore, the temperature used in this study had to be as low as possible, so 35 °C was used for the experiments.

The optimized synthetic conditions for P(AM/NaAA/AQAS1) were 35 wt% total monomer content, 0.5 mol% modified monomer content, 0.3 wt% initiator, 1 wt% urea, 35 °C. Similarly, the optimized synthetic conditions for P(AM/NaAA/AQAS2) were 35 wt% total monomer content, 0.25 mol% modified monomer content, 0.1 wt% initiator, 1 wt% urea, 35 °C.

The intrinsic viscosities [η] of HPAM, P(AM/NaAA/AQAS1), and P(AM/NaAA/AQAS2) were 200.87, 477.20, and 754.14 mL/g, respectively. Then, Eq. (1) was used to calculate the molecular weights of the copolymers; the molecular weight of M_{wHPAM} was 6.06×10^5 , that of $M_{\text{wP(AM/NaAA/AQAS1)}}$ was 1.79×10^6 , and that of $M_{\text{wP(AM/NaAA/AQAS2)}}$ was 3.17×10^6 . The molecular weights of the hydrophobically associative polymers are similar to those reported in the research (2.21×10^6) (Jing et al., 2019).

3.3. Critical association concentrations and fluorescence spectra of the copolymers

Copolymers may present different properties for different hydrophobic associating structures. The critical association concentration (CAC) can be determined from the relationship between the apparent viscosity and the copolymer concentration. The CAC indicates whether the hydrophobic groups participated effectively in the formation of the intermolecular associated structure. As shown in Fig. 5(b), the viscosity of the P(AM/NaAA/AQAS2) solution increased slowly when the concentration was below 4000 mg/L; when the concentration was increased from 4000 to 5000 mg/L, the viscosity rose sharply, and intermolecular association occurred at this time. In contrast, P(AM/NaAA/AQAS1) had no obvious critical

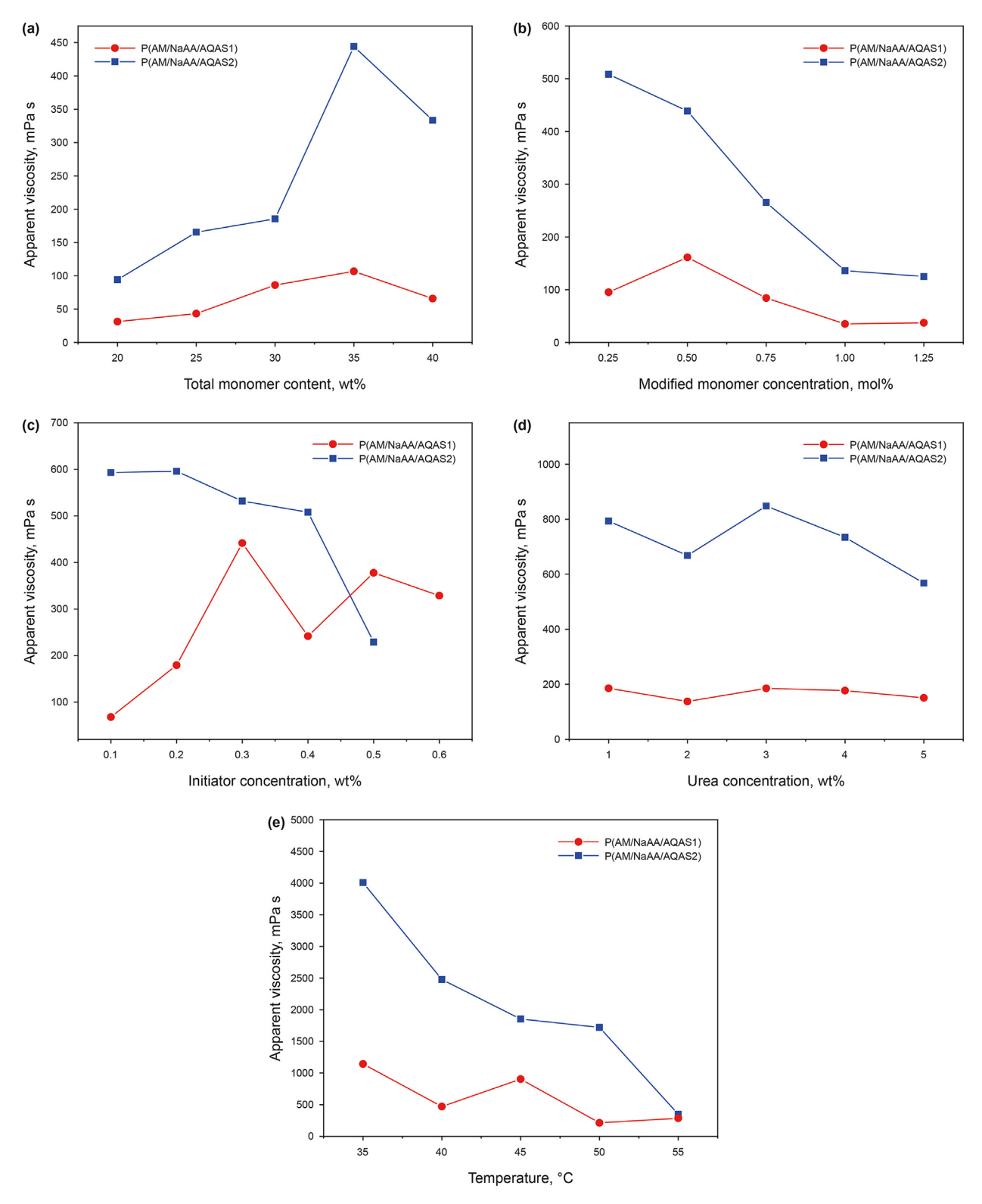


Fig. 4. Effects of synthetic conditions on the apparent viscosities.

association concentration within the concentration range 1000–7000 mg/L. Most likely, the modified monomer chain segments were too short and had not reached the critical association concentration within the measurement range. This experiment showed that the copolymer with the linear chain structure had stronger hydrophobic interactions than the copolymer with a ring

structure based on the same number of carbon atoms.

The hydrophobic association effects of P(AM/NaAA/AQAS2) were investigated with fluorescence spectroscopy (Fig. 6). The fluorescence intensity of pyrene in the copolymer solution first increased and then decreased with increasing concentration. The I_1/I_3 value for a 20 mg/L concentration was 1.51, and the I_1/I_3 for a

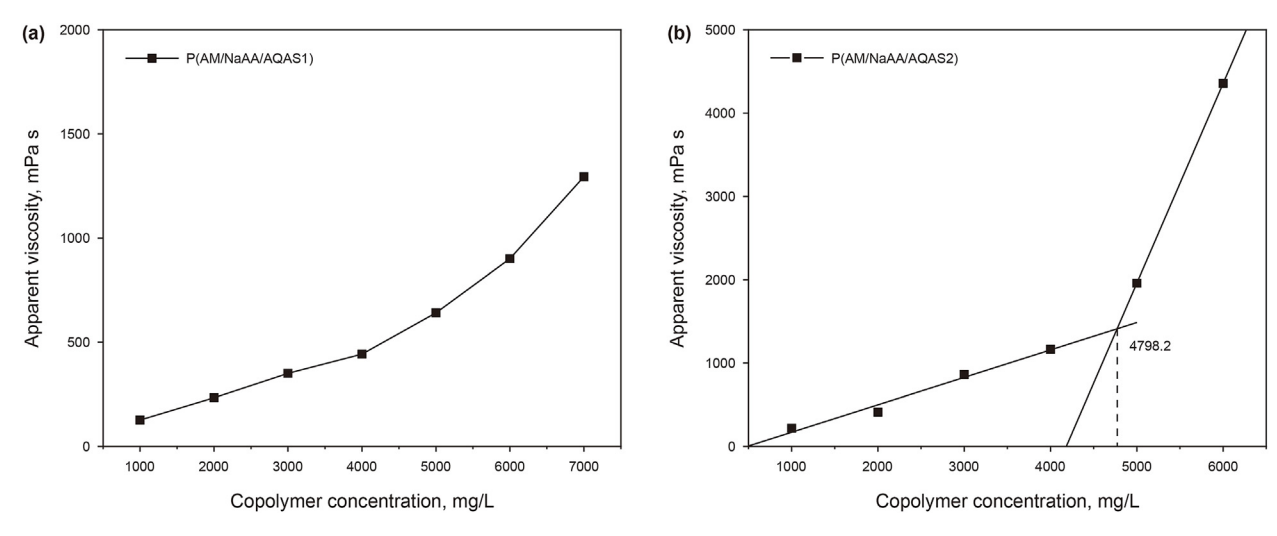


Fig. 5. Variations in the apparent viscosities of the copolymer solutions with concentration.

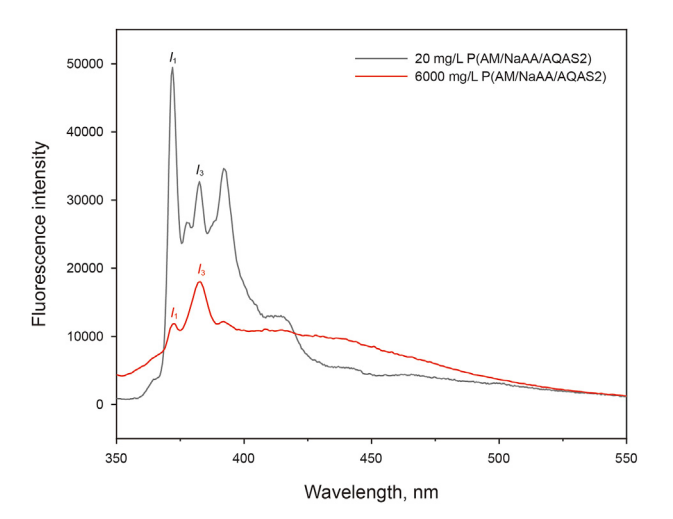


Fig. 6. Fluorescence spectra of pyrene in P(AM/NaAA/AQAS2) solutions with different mass fractions.

6000 mg/L concentration was 0.66. From 20 to 6000 mg/L, the value decreased by 0.85, which indicated that when the concentration exceeded the CAC, hydrophobic microdomains were formed.

3.4. Micromorphologies of the polymer solutions

SEM was utilized to investigate the micromorphologies of the copolymer solutions, Fig. 7(c) and (d) shows that the networks in P(AM/NaAA/AQAS2) were tighter than those in HPAM, meanwhile, Fig. 7(a) and (b) exhibits the same phenomenon, the results show that the hydrophobic groups in the modified polymer may form an association structure, resulting in a tighter network. The networks in Fig. 7(e) were more compact than those in Fig. 7(d), which meant that above the CAC, intermolecular association occurred instead, or it could be caused by high concentrations of P(AM/NaAA/AQAS2). As shown in Fig. 7(a) and (c), the HPAM polymer chains are entangled in the aqueous solution, but the entanglement is less dense than the network structure formed by the modified polyacrylamide. This may be due to the absence of hydrophobic modifying groups in HPAM, which do not form an associative structure.

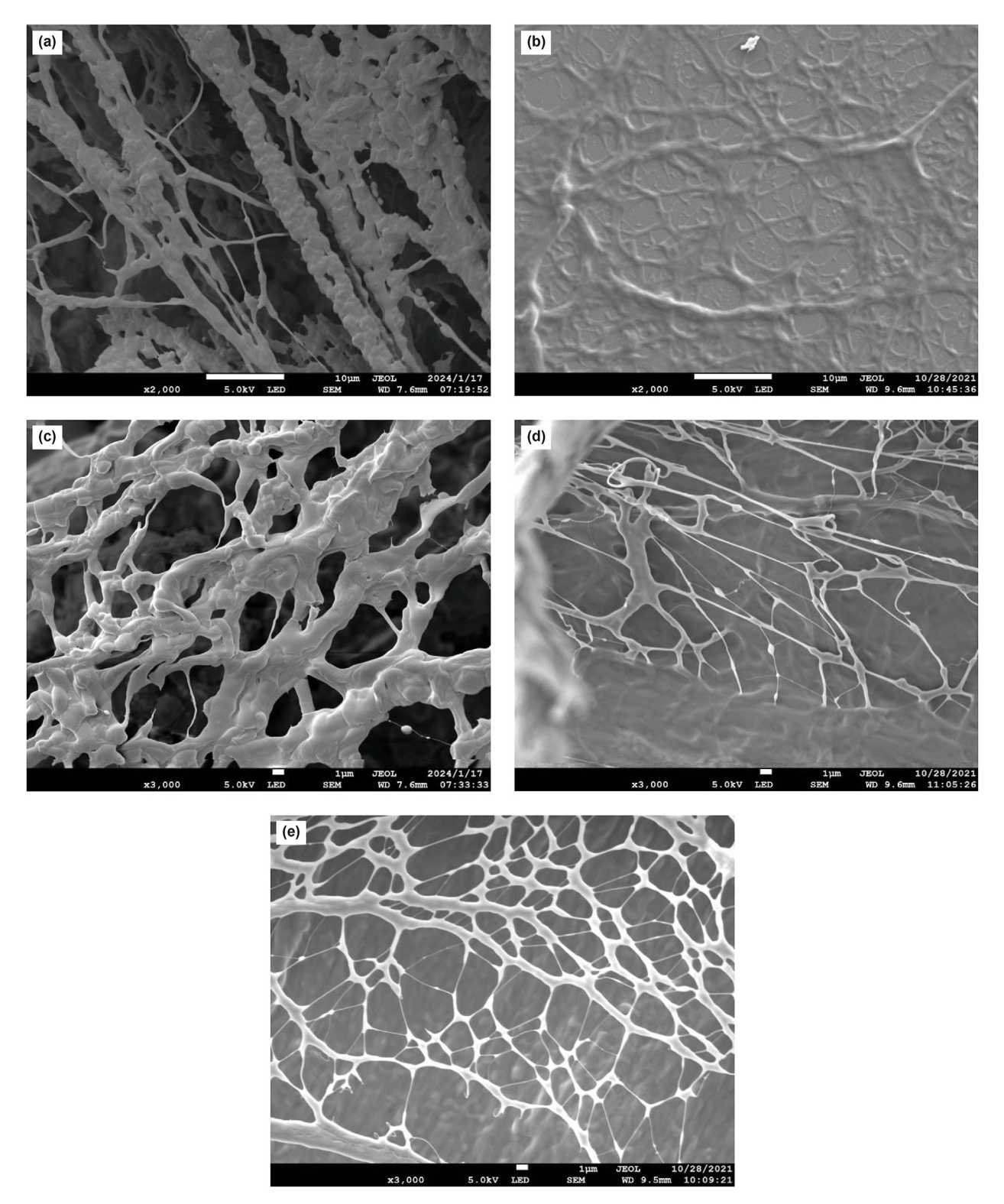
3.5. Properties of the copolymer solutions

3.5.1. Salt and shear sensitivity tests

The salt tolerance values of the copolymer solutions (3000 mg/L) were studied at room temperature with a Brookfield DV2T viscometer (ULA [0] rotor), and the results are shown in Fig. 8. The apparent viscosities of the P(AM/NaAA/AQAS1) and P(AM/NaAA/AQAS2) solutions were both higher than that of HPAM in fresh water. When the concentration of NaCl was increased to 10,000 mg/L, the apparent viscosities for P(AM/NaAA/AQAS1) and P(AM/NaAA/AQAS2) were 9.54 and 13.8 mPa s, respectively, and both copolymer viscosities were higher than that of HPAM. P(AM/NaAA/AQAS2) had a higher initial viscosity and exhibited better salt tolerance, which may indicate that the linear chains easily associated with each other to form a network.

Two methods were used to test the shear resistances of the copolymer solutions (3000 mg/L) at room temperature with an MCR102 Anton Paar rheometer. In the first method, the shear rate was maintained at 170 s⁻¹ and viscosity changes were determined after 60 min; in the second measurement method, when the shear rate was gradually increased from 1 to 1000 s^{-1} , the changes of the polymer viscosity was measured after shearing 30 min. The results are shown in Fig. 9. The viscosity retention rates for HPAM, P(AM/ NaAA/AQAS1) and P(AM/NaAA/AQAS2) were 98.4%, 85.0% and 101.4% (Fig. 9(a)), respectively. When the shear rate was raised from 170 to 1000 s^{-1} , the viscosities of the copolymers decreased dramatically (Fig. 9(b)). The viscosities of HPAM, P(AM/NaAA/ AQAS1) and P(AM/NaAA/AQAS2) were 19.9, 21.4, and 23.7 mPa s, respectively. Comparing the rheological properties of the three polymers, it is evident from Fig. 9(b) that the apparent viscosity of all three polymers decreases with increasing shear rate (from 0 to 1000 s⁻¹). However, it is worth noting that in aqueous solution, the viscosity of the three polymers follows the trend P(AM/NaAA/ AQAS2) > P(AM/NaAA/AQAS1) > HPAM, in the shear rate range of $17.9-1000 \text{ s}^{-1}$ (second point to the last point). This perhaps indicated that the linear chains improved the shear resistance and apparent viscosity of the polymer beyond those of the cyclic structure, which showed that the viscosities of both copolymer solutions were retained under shearing. Because AQAS2 has a straight-chain structure, the sigma bond can undergo internal rotation. In the aqueous solution, it can easily twist into a conformation where hydrophobic association can occur. However, the conjugated structure of the rigid benzene ring restricts the internal

Y.-X. Dai, X.-L. Zhang, S.-Y. Liu et al. Petroleum Science 21 (2024) 1889–1901



 $\begin{array}{l} \textbf{Fig. 7.} \ \ \text{SEM images of HPAM (2000 mg/L,} \times 2000) \textbf{ (a)}, P(AM/NaAA/AQAS1) (2000 mg/L,} \times 2000) \textbf{ (b)}; HPAM (2000 mg/L,} \times 3000) \textbf{ (c)}, P(AM/NaAA/AQAS2) (2000 mg/L,} \times 3000) \textbf{ (d)}, \\ \text{and } P(AM/NaAA/AQAS2) (5000 mg/L,} \times 3000) \textbf{ (e)}. \end{array}$

rotation of the sigma bonds, preventing the formation of more associative conformations, unlike the chain structure, this difference results in a variation in rheological properties.

3.5.2. Viscoelasticity of copolymers

The rheological properties of the copolymers were used to

evaluate the elasticities and viscosities of the fluids. The elastic modulus (G') and viscous modulus (G'') were used to represent the rheological properties (Rodríguez-Rivero et al., 2014).

As shown in Fig. 10, the elastic modulus (G') of P(AM/NaAA/AQAS1) was higher than the viscous modulus (G'') when the copolymer concentration was 1000 mg/L, but as the concentration

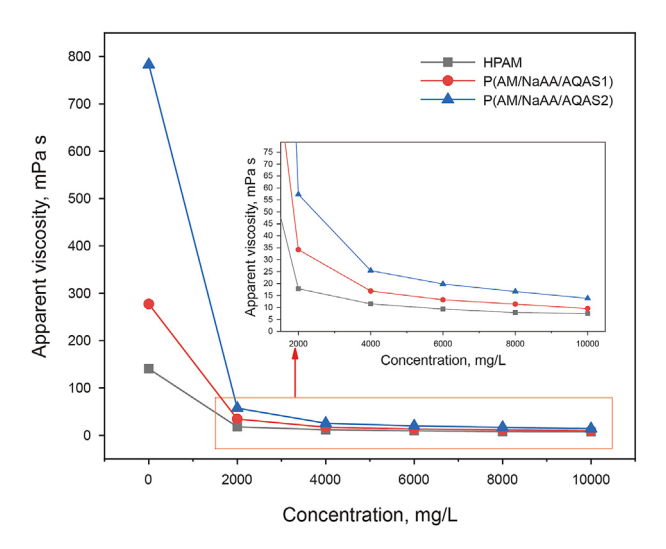


Fig. 8. Salt tolerance of the copolymers and HPAM solution.

was increased, the elastic modulus (G') and viscous modulus (G'') curves almost overlapped at 5000 mg/L, and if the concentration was increased continuously, a more compact network structure should be formed, the elastic modulus (G') should be higher than the viscous modulus (G'') and indicate elasticity.

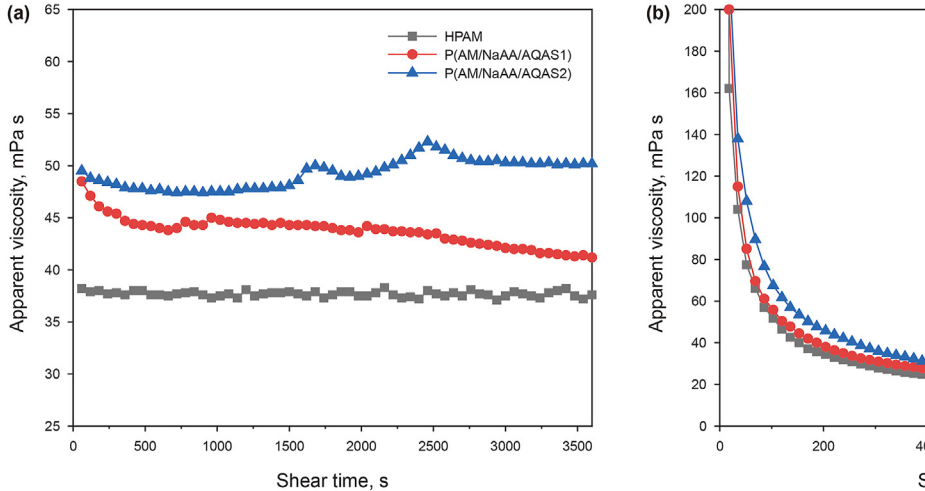
Fig. 11 shows that the elastic modulus (G') and the viscous modulus (G'') both increased with increasing concentration from 1000 to 5000 mg/L. The elastic modulus (G') of P(AM/NaAA/AQAS2) almost reached the viscous modulus (G') at 1000 mg/L when the strain ranged from 0.1% to 100%. Moreover, as the concentration was increased, the elastic modulus (G') became higher than the viscous modulus (G'') at 3000 mg/L, and the elastic modulus (G') eventually became significantly higher than the viscous modulus (G''). The elastic modulus (G') was significantly higher than the viscous modulus (G'') at 3000 mg/L and in the range of 1–10 rad/s. Based on the viscoelastic theory of drag reduction agents, the polymer was a low-viscosity high-elasticity fluid at concentrations greater than 3000 mg/L.

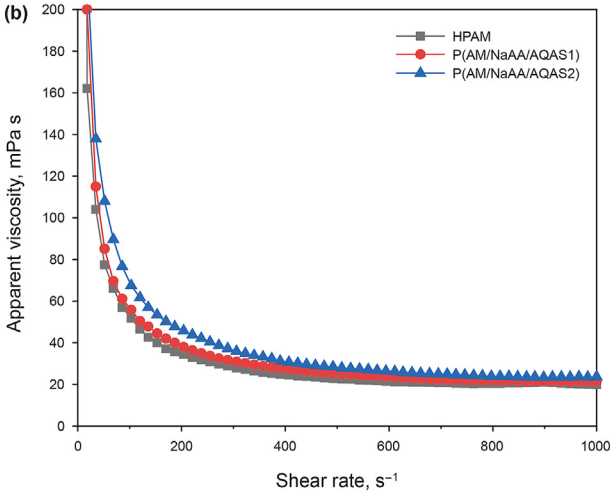
3.5.3. Drag reduction performance

As shown in Fig. 12, the DR rates of the copolymers both increased with increasing flow rate. When the concentrations of

P(AM/NaAA/AOAS1) were 500, 1000, and 1500 mg/L, and the flow rate was 20 L/min, the DR rates were 69%, 73.6%, and 72.8%, respectively. As the flow rate increased, P(AM/NaAA/AQAS1) exhibited excellent drag reduction performance, when the flow rate was 45 L/min, the DR rates of different concentrations of P(AM/ NaAA/AQAS1) reached 71.6%, 75.8%, and 77.9%. These results showed that the DR rate exceeded 75% when the copolymer concentration was 1000 mg/L. Obviously, the DR rate of P(AM/NaAA/ AQAS2) decreased as the concentration was increased at a low flow rate, which could have been caused by the continuous increases in the concentration of P(AM/NaAA/AQAS2); the viscosity of the solution was extremely high, which increased the frictional resistance of the fluid in the pipeline. When the flow rate was increased to 45 L/min, the DR rates of three different concentrations (500, 1000, and 1500 mg/L) of P(AM/NaAA/AQAS2) reached 75.2%, 76.5% and 75.2%, respectively, and when the concentration was 500 mg/L, a high DR rate was achieved. Both of the copolymers exhibited excellent DR performance in fresh water.

In field applications, large amounts of water are needed for the shale gas fracture processes, but fresh water is not easily obtained, and the use of fresh water is not sustainable. Therefore, salty formation water and fracturing flowback fluid should be utilized appropriately. 10,000 mg/L NaCl solution was prepared to simulate brine. As shown in Fig. 13, the DR rates of P(AM/NaAA/AQAS1) and P(AM/NaAA/AQAS2) were both higher than the DR rate of HPAM at the same concentrations. When the concentration of P(AM/NaAA/ AOAS1) and HPAM was 1000 mg/L, and the concentration of P(AM/ NaAA/AOAS2) and HPAM was 500 mg/L, at low flow rates, the DR rates of the copolymers were maintained above 70%, and the DR rates of HPAM were 33.6% and 29.9%, respectively, when the flow rate reached 45 L/min, the DR rates of the copolymers were approximately 73.0%, under the same test conditions, the DR rates of HPAM were 45.0% and 43.2%. This indicated that the brine did not affect the copolymer DR performance significantly, and the DR performance was better than that of HPAM. It is noteworthy that, while the concentration of P(AM/NaAA/AQAS1) was 1000 mg/L and the concentration of P(AM/NaAA/AQAS2) was 500 mg/L, the lowest DR rate of P(AM/NaAA/AQAS1) was 70.12% and that of P(AM/NaAA/ AQAS2) was 71.29% at 10,000 mg/L brine. At the same brine conditions, the research (Wang et al., 2016) demonstrated that the maximum drag reduction rate could reach approximately 65% when the mass fraction of the drag reduction agent was 0.2%. P(AM/ NaAA/AQAS1) and P(AM/NaAA/AQAS2) exhibited the advantage of





 $\textbf{Fig. 9.} \ \ \textbf{Shear resistances of the copolymers and HPAM solution}.$

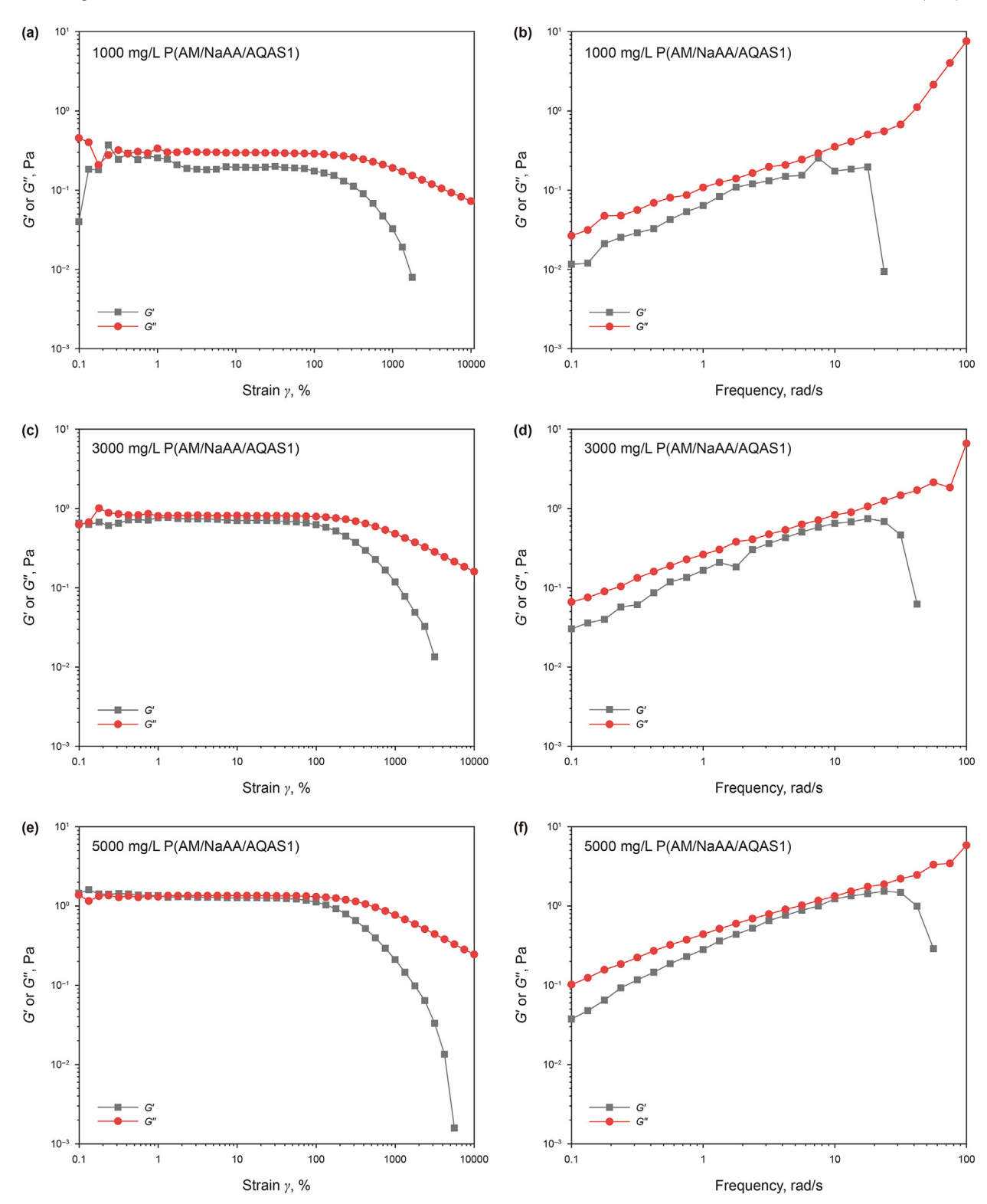


Fig. 10. Viscoelasticity of P(AM/NaAA/AQAS1) solutions of different concentrations.

higher DR rate at lower dosages compared to the drag reducers mentioned in the research.

Fig. 13 also shows that P(AM/NaAA/AQAS1) and P(AM/NaAA/AQAS2) exhibit good drag reduction ability in brine (10,000 mg/L). This is attributed to the addition of cyclic and chain quaternary ammonium salt modified monomers, which enhance the drag

reduction performance of the polymers. However, there is not a significant difference in the drag reduction performance. This could be attributed to the hydrophobic structure of both modified monomers. This structure can increase the shear resistance of the drag-reducing agent and inhibit turbulence, thereby enhancing its drag-reducing effect.

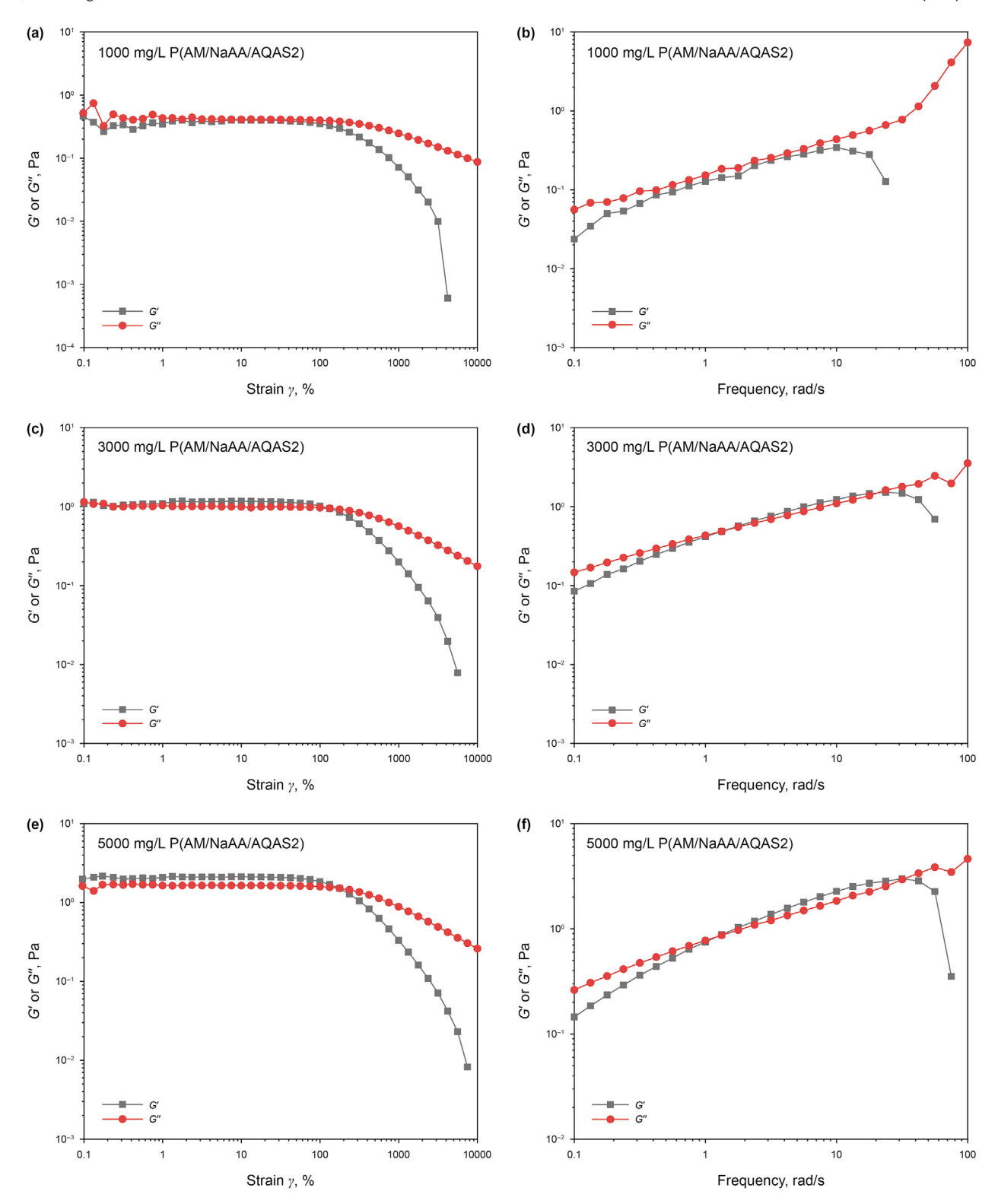


Fig. 11. Viscoelasticity of P(AM/NaAA/AQAS2) solutions of different concentrations.

The drag reduction rate of modified polyacrylamide is significantly higher than that of HPAM under the same conditions. The reasons may be as follows. (1) The modified polyacrylamide is less affected by salt ions in saline solution, and the molecular chain is not easy to be curled, which improves the salt resistance of the drag reducing agent. (2) In the case of high flow rate, the polymer

molecular chain is very easy to be fractured by shear, and due to the addition of modified monomers, it allows the modified polyacrylamide to intertwine with each other to a higher degree in the aqueous solution than HPAM, and the network structure is more complete and densely packed. After shearing, the modified polymer will re-connect due to the presence of hydrophobic groups. This

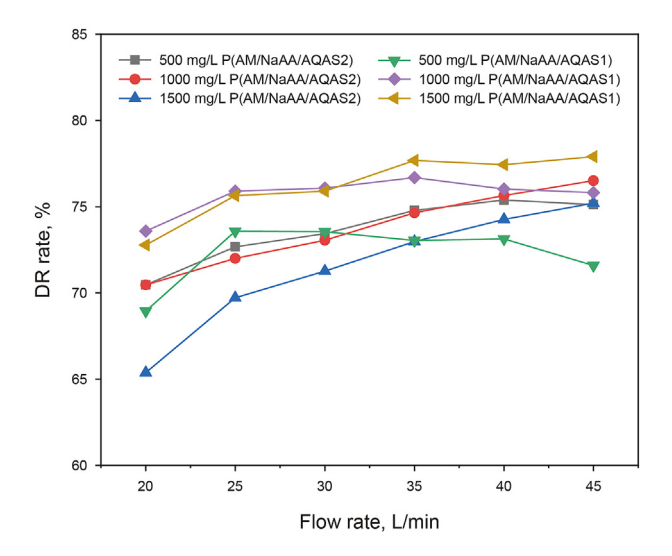


Fig. 12. Drag reduction rates of the copolymers in fresh water.

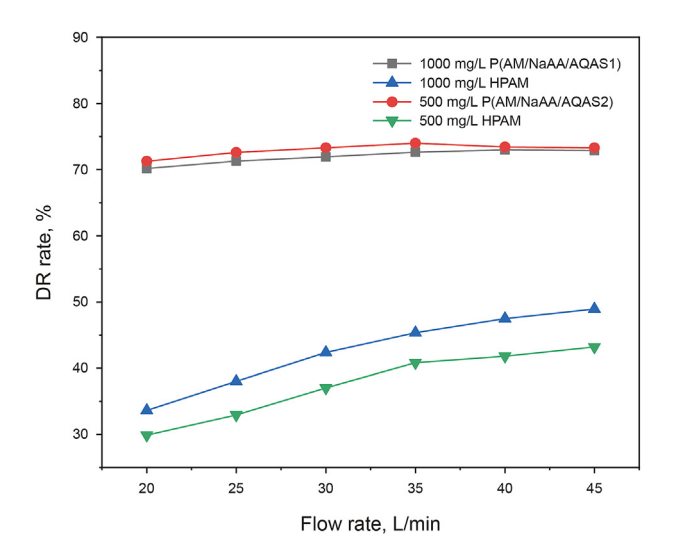


Fig. 13. Drag reduction rates of the copolymers and HPAM in brine.

connected structure enhances the viscosity of the polymer solution and inhibits turbulence in the pipeline, thereby enhancing the drag-reducing effect of the modified polyacrylamide.

In contrast, HPAM in aqueous solution relies solely on its own carbon chain. In cases of high flow velocity in the pipeline, this can cause the HPAM molecular chain to be broken by shearing. There are no hydrophobic monomers that can reconnect to the structure, resulting in poor drag reduction performance.

4. Conclusions

In this paper, two hydrophobic associating drag reduction agents were reported. Appropriate synthetic conditions, property tests of copolymer solutions, such as salt tolerance and shear resistance, rheology, and the drag reduction performance, were investigated. The following conclusions were drawn.

(1) The two products showed better salt tolerance than HPAM; compared with that of P(AM/NaAA/AQAS1), P(AM/NaAA/AQAS2) presented a higher salt tolerance, which meant that the linear chain structure was more effective in overcoming

- the negative effects of NaCl and more easily formed a network structure. This indicated that the linear chain structure engaged in hydrophobic association more readily than the ring structure.
- (2) The shear resistances and rheology were determined with an MCR102 Anton Paar rheometer. The viscosity retention rate of P(AM/NaAA/AQAS1) was approximately 85.0%, and that of P(AM/NaAA/AQAS2) was 100% after shearing for 60 min at 170 s⁻¹. The viscosities of P(AM/NaAA/AQAS1) and P(AM/NaAA/AQAS2) were 21.4 and 23.7 mPa s at 1000 s⁻¹, respectively. The rheological properties of the copolymer solutions were characterized. At a concentration of 3000 mg/L, P(AM/NaAA/AQAS2) exhibited an elastic modulus (*G'*) higher than the viscous modulus (*G''*). However, 5000 mg/L P(AM/NaAA/AQAS1) did not show the same behavior. Based on viscoelastic theory, the linear chain structure showed good shear resistance and a high sand-carrying capacity.
- (3) With the same test conditions, both of these products showed high drag reductions. In fresh water, when the flow rate was 45 L/min, the drag reduction rate of 1000 mg/L P(AM/NaAA/AQAS1) was approximately 75.8%, and 500 mg/L P(AM/NaAA/AQAS1) presented a 75.2% drag reduction rate. In brine, the drag reduction rates for 1000 mg/L P(AM/NaAA/AQAS1), 500 mg/L P(AM/NaAA/AQAS2), 1000 mg/L HPAM, and 500 mg/L HPAM were 72.9%, 73.3%, 43.2% and 49.0%, respectively. P(AM/NaAA/AQAS1) and P(AM/NaAA/AQAS2) exhibited excellent drag reductions, and their application in the field is expected.

CRediT authorship contribution statement

Ya-Xing Dai: Writing — review & editing, Writing — original draft, Validation, Investigation, Formal analysis. Xian-Li Zhang: Visualization, Methodology, Formal analysis. Si-Yuan Liu: Supervision, Conceptualization. Feng-Run-Ze Zhang: Validation, Formal analysis. Yi-Xi Zhang: Visualization, Investigation. Yu-Tong Sang: Methodology, Conceptualization. Jing-Xi Zheng: Methodology, Conceptualization. Zhao-Sheng Liu: Project administration. Peng Zhang: Writing — review & editing, Supervision, Investigation, Funding acquisition, Formal analysis.

Declaration of competing interest

The authors declare that they have no known competing financial interests or personal relationships that could have appeared to influence the work reported in this paper.

Acknowledgements

This work was supported by the National Natural Science Foundation of China (Project Nos. 51774062 and 52274032), Scientific and Technological Key Research Program of Chongqing Municipal Education Commission (KJZD-K201901502), General Project of Chongqing Natural Science Foundation (CSTB2022NSCQ-MSX0349), and Science and Technology Research Program of Chongqing Municipal Education Commission (KJQN202313101).

References

Chen, H., Liu, H.Z., Zhang, S., Feng, Y.J., 2020. Smart thermoviscosifying polymer for improving drag reduction in slick-water hydrofracking. Fuel 278, 118408. https://doi.org/10.1016/j.fuel.2020.118408.

Chen, P., Chang, H., Peng, T., Tang, Y., Liu, Y., Xiang, C., 2021. Synthesis and performance evaluation of a new drag reducer based on acrylamide/12-allyloxydodecyl acid sodium. J. Appl. Polym. Sci. 138 (30), 50314. https://

doi.org/10.1002/app.50314.

- Dai, X.D., Li, B., Li, L., Yin, S.M., Wang, T., 2021. Experimental research on the characteristics of drag reduction and mechanical degradation of polyethylene oxide solution. Energy Sources, Part A Recovery, Util. Environ. Eff. 43 (8), 944–952. https://doi.org/10.1080/15567036.2019.1632988.
- Gu, Y.Q., Yu, S.W., Mou, J.G., Wu, D.H., Zheng, S.H., 2020. Research progress on the collaborative drag reduction effect of polymers and surfactants. Materials 13 (2), 444. https://doi.org/10.3390/ma13020444.
- Ge, Y.R., Zhao, Z.C., Cheng, X.L., Chen, T.F., Liu, T., Guo, X.P., 2021. Research of a novel double cross-linking fracturing fluid. J. Pet. Explor. Prod. Technol. 11 (5), 2191–2197. https://doi.org/10.1007/s13202-021-01167-5.
- Guo, H., 2021. Synthesis and evaluation of new slickwater fracturing fluid for drag reduction. IOP Earth Environ. Sci. 651 (3), 032082. https://doi.org/10.1088/1755-1315/651/3/032082.
- Habibpour, M., Clark, P.E., 2017. Drag reduction behavior of hydrolyzed polyacrylamide/xanthan gum mixed polymer solutions. Petrol. Sci. 14 (2), 412–423. https://doi.org/10.1007/s12182-017-0152-7.
- Ibrahim, A., Nasr-El-Din, H., Rabie, A., Lin, G., Zhou, J., Qu, Q., 2018. A new friction-reducing agent for slickwater-fracturing treatments. SPE Prod. Oper. 33 (3), 583–595. https://doi.org/10.2118/180245-PA.
- Jing, X., Liu, Y., Li, W., Xu, Y., Huang, Z., 2019. Using water-miscible nonionic hydrophobic monomer associating HPAM as drag reducing agent. J. Appl. Polym. Sci. 136 (48), 48362. https://doi.org/10.1002/app.48362.
- Jing, X., Huang, C., Fu, Z., 2021. Synthesis and performance evaluation of a new drag reducer—cationic hybrid polymeric based on polyacrylamide. J. Polym. Res. 28 (11), 435. https://doi.org/10.1007/s10965-021-02701-7.
- Kerimov, V.Y., Mustaev, R., Bondarev, A., 2016. Evaluation of the organic carbon content in the low-permeability shale formations (as in the case of the Khadum suite in the Ciscaucasia region). Orient. J. Chem. 32 (6), 3235–3241. https:// doi.org/10.13005/ojc/320648.
- Kim, O., Little, R., Patterson, R., Ting, R., 1974. Polymer structures and turbulent shear stability of drag reducing solutions. Nature 250 (5465), 408–410. https:// doi.org/10.1038/250408a0.
- Li, Q., Wang, F.L., Forson, K., Zhang, J.Y., Zhang, C.L., Chen, J., Xu, N., Wang, Y.L., 2022a. Affecting analysis of the rheological characteristic and reservoir damage of CO₂ fracturing fluid in low permeability shale reservoir. Environ. Sci. Pollut. Control Ser. 29 (25), 37815—37826. https://doi.org/10.1007/s11356-021-18169-9.
- Ser. 29 (25), 37815–37826. https://doi.org/10.1007/s11356-021-18169-9. Li, Q., Wang, F.L., Wang, Y.L., Zhang, J.Y., Yu, X.Q., Zhao, M., Zhou, C., Forson, K., Shi, S., Zhao, Y., Li, W.S., 2022b. Influence of organoboron cross-linker and reservoir characteristics on filtration and reservoir residual of guar gum fracturing fluid in low-permeability shale gas reservoirs. Environ. Sci. Pollut. Control Ser. 29 (55), 82975–82985. https://doi.org/10.1007/s11356-022-21577-0.
- Lin, Z., Zakin, J.L., Zheng, Y., Davis, H.T., Scriven, L., Talmon, Y., 2001. Comparison of the effects of dimethyl and dichloro benzoate counterions on drag reduction, rheological behaviors, and microstructures of a cationic surfactant. J. Rheol. 45 (4), 963–981. https://doi.org/10.1122/1.1380261.
- Ma, G.Y., Li, X.R., Wang, X.R., Liu, G.J., Jiang, L., Yang, K., 2019. Preparation, rheological and drag reduction properties of hydrophobically associating polyacrylamide polymer. J. Dispersion Sci. Technol. 40 (2), 171–178. https://doi.org/10.1080/01932691.2018.1461637.
- Nakamura, H., Iwamori, H., Nakagawa, M., Shibata, T., Kimura, J.I., Miyazaki, T., Chang, Q., Vaglarov, B.S., Takahashi, T., Hirahara, Y., 2019. Geochemical mapping of slab-derived fluid and source mantle along Japan arcs. Gondwana Res. 70,

- 36-49. https://doi.org/10.1016/j.gr.2019.01.007.
- Nguyen, T.C., Romero, B., Vinson, E., Wiggins, H., 2018. Effect of salt on the performance of drag reducers in slickwater fracturing fluids. J. Petrol. Sci. Eng. 163, 590–599. https://doi.org/10.1016/j.petrol.2018.01.006.
- Pu, W.F., Du, D.J., Liu, R., Gu, J.Y., Li, K.W., Zhang, Y.Y., Liu, P.G., 2016. Synthesis and characterization of hyperbranched associative polyacrylamide. RSC Adv. 6 (45), 39522–39529. https://doi.org/10.1039/c6ra05243f.
- Rodríguez-Rivero, C., Hilliou, L., Martín del Valle, E.M., Galán, M.A., 2014. Rheological characterization of commercial highly viscous alginate solutions in shear and extensional flows. Rheol. Acta 53, 559–570. https://doi.org/10.1007/s00397-014-0780-4.
- dos Santos, W.R., Caser, E.S., Soares, E.J., Siqueira, R.N., 2020. Drag reduction in turbulent flows by diutan gum: a very stable natural drag reducer. J. Non-Newtonian Fluid Mech. 276, 104223. https://doi.org/10.1016/j.jnnfm.2019.104223.
- Soares, E.J., 2020. Review of mechanical degradation and de-aggregation of drag reducing polymers in turbulent flows. J. Non-Newtonian Fluid Mech. 276, 104225. https://doi.org/10.1016/j.jnnfm.2019.104225.
- Tamano, S., Itoh, M., Kato, K., Yokota, K., 2010. Turbulent drag reduction in nonionic surfactant solutions. Phys. Fluids 22 (5), 055102. https://doi.org/10.1063/1.3407666.
- Tan, H.Z., Mao, J.C., Zhang, W.L., Yang, B., Yang, X.J., Zhang, Y., Lin, C., Feng, J.F., Zhang, H., 2020. Drag reduction performance and mechanism of hydrophobic polymers in fresh water and brine. Polymers 12 (4), 955. https://doi.org/ 10.3390/polym12040955.
- Tian, M., Fang, B., Jin, L.P., Lu, Y.J., Qiu, X.H., Jin, H., Li, K.J., 2015. Rheological and drag reduction properties of hydroxypropyl xanthan gum solutions. Chin. J. Chem. Eng. 23 (9), 1440–1446. https://doi.org/10.1016/j.cjche.2015.04.003.
- Wang, L., Wang, D., Shen, Y.D., Lai, X.J., Guo, X., 2016. Study on properties of hydrophobic associating polymer as drag reduction agent for fracturing fluid. J. Polym. Res. 23 (8), 235. https://doi.org/10.1007/s10965-016-1129-8.
- Wei, J.M., Jia, W.F., Zuo, L., Chen, H., Feng, Y.J., 2022. Turbulent drag reduction with an ultra-high-molecular-weight water-soluble polymer in slick-water hydrofracking. Molecules 27 (2), 351. https://doi.org/10.3390/molecules27020351.
- Xing, J., Wu, A., Shu, W., Zhang, Y., Li, Y., Yu, W., 2020. Laboratory research on the performance of fracturing fluid system for unconventional oil and gas reservoir transformation. Open J. Yangtze Oil Gas 5 (4), 176–187. https://doi.org/10.4236/ojogas.2020.54014.
- Yang, B., Zhao, J.Z., Mao, J.C., Tan, H.Z., Zhang, Y., Song, Z.F., 2019. Review of friction reducers used in slickwater fracturing fluids for shale gas reservoirs. J. Nat. Gas Sci. Eng. 62, 302—313. https://doi.org/10.1016/j.jngse.2018.12.016.

 Yu, H.Y., Ma, Z.F., Tang, L., Li, Y.S., Shao, X.Z., Tian, Y.X., Qian, J., Fu, J., Li, D., Wang, L.,
- Yu, H.Y., Ma, Z.F., Tang, L., Li, Y.S., Shao, X.Z., Tian, Y.X., Qian, J., Fu, J., Li, D., Wang, L., Ren, F.G., 2022. The effect of shear rate on dynamic gelation of phenol formaldehyde resin gel in porous media. Gels 8 (3), 185. https://doi.org/10.3390/gels8030185
- Zeng, Q., Fu, P., Meng, L., Shi, H., Zhou, H., Yu, W., 2020. Research and application of an environmental-friendly low-damage and high salt-resistance slick water fracturing fluid system. Open J. Yangtze Oil Gas 5 (3), 131–143. https://doi.org/ 10.4236/ojogas.2020.53011.
- Zhao, J.Z., Chen, P.F., Liu, Y.Q., Zhao, W.W., Mao, J.C., 2018. Prediction of field drag reduction by a modified practical pipe diameter model. Chem. Eng. Technol. 41 (7), 1417–1424. https://doi.org/10.1002/ceat.201600570.